Combined Radiometer-Radar Microphysical Profile Estimations with Emphasis on High Frequency Brightness Temperature Observations

Gail Skofronick Jackson[1,2], James R. Wang[2], Gerald M. Heymsfield[3], Robbie Hood[4], Will Manning[1], Robert Meneghini[2], James A. Weinman[2,5]

[1]University of Maryland, Baltimore County
Goddard Earth Sciences and Technology Center
NASA Goddard, Code 975, Bldg. 33, Room A428, Greenbelt, MD 20771
301-614-5720, FAX 301-614-5558, gailsjackson@ieee.org

[2]NASA Goddard Space Flight Center, Code 975, Greenbelt, MD 20771
[3]NASA Goddard Space Flight Center, Code 912, Greenbelt, MD 20771
[4]NASA Marshall Space Flight Center, SD60, Huntsville, AL 35812
[5]Department of Atmospheric Science, University of Washington, Seattle, WA 98195

To be submitted to the Journal of Applied Meteorology, December 2001

Popular Summary

Profiles of hydrometeor characteristics were estimated using an iterative retrieval algorithm. The algorithm minimized the differences between forward calculations and observed radar and radiometer observations from the ER-2 aircraft obtained during CAMEX-3. The advantages of this retrieval algorithm are the use of high frequency channels (89 to 340 GHz) to provide details of the frozen hydrometeors and combining radar and radiometer observations.

The retrieval was performed on anvil, convective, and quasi-stratiform cloud types associated with the outer eyewalls of Hurricane Bonnie (August 1998). The retrieval results were qualitatively validated using observations from two independent measurements observing the same scene. The validation data corroborated the retrieved contents and particle size distributions.

This work shows the importance of including the high frequencies when attempting to estimate frozen hydrometeor characteristics using radar and radiometer data. Indeed, neglecting the high frequencies yielded acceptable estimates of the liquid profiles, but the ice profiles were poorly retrieved. The retrieved profiles contain considerable information about the cloud structure and hydrometeor size distributions even though they may not have unique solutions. The retrieved profiles are important for improving global change models and cloud resolving models.

Combined Radiometer-Radar Microphysical Profile Estimations with Emphasis on High Frequency Brightness Temperature Observations

Gail Skofronick Jackson[1,2], James R. Wang[2], Gerald M. Heymsfield[3], Robbie Hood[4], Will Manning[1], Robert Meneghini[2], James A. Weinman[2,5]

[1]University of Maryland, Baltimore County
Goddard Earth Sciences and Technology Center
NASA Goddard, Code 975, Bldg. 33, Room A428, Greenbelt, MD 20771
301-614-5720, FAX 301-614-5558, gailsjackson@ieee.org

[2]NASA Goddard Space Flight Center, Code 975, Greenbelt, MD 20771
[3]NASA Goddard Space Flight Center, Code 912, Greenbelt, MD 20771
[4]NASA Marshall Space Flight Center, SD60, Huntsville, AL 35812
[5]Department of Atmospheric Science, University of Washington, Seattle, WA 98195

To be submitted to the Journal of Applied Meteorology, December 2001

Abstract

Information about the vertical microphysical cloud structure is useful in many modeling and predictive practices. Radiometers and radars are used to observe hydrometeor properties. This paper describes an iterative retrieval algorithm that combines the use of airborne active and wideband (10 to 340 GHz) passive observations to estimate the vertical content and particle size distributions of liquid and frozen hydrometeors. The physically-based retrieval algorithm relies on the high frequencies (> 89 GHz) to provide details on the frozen hydrometeors. Neglecting the high frequencies yielded acceptable estimates of the liquid profiles, but the ice profiles were poorly retrieved. Airborne radar and radiometer observations from the third Convection and Moisture EXperiment (CAMEX-3) were used in the retrieval algorithm as constraints. Nadir profiles were estimated for a minute each of flight time (approximately 12.5 km along track) from an anvil, convection, and quasi-stratiform rain. The complex structure of the frozen hydrometeors required the most iterations for convergence for the anvil cloud type. The wideband observations were found to more than double the estimated frozen hydrometeor content as compared to retrievals using only 90~GHz and below. The convective and quasi-stratiform quickly reached convergence (minimized difference between observations and calculations using the estimated profiles). A qualitative validation using coincident in situ CAMEX-3 observations shows that the retrieved particle size distributions are well corroborated with independent measurements.

Combined Radiometer-Radar Microphysical Profile Estimations with Emphasis on High Frequency Brightness Temperature Observations

Gail M. Skofronick-Jackson[1], James R. Wang[2], Gerald M. Heymsfield[2], Robbie Hood[3], Will Manning[1], Robert Meneghini[2], James A. Weinman[2]

[1]University of Maryland, Baltimore County
Goddard Earth Sciences and Technology Center
NASA Goddard, Code 975, Bldg. 33, Rm. A428
Greenbelt, MD 20771

[2]NASA Goddard Greenbelt, MD 20771

[3]NASA Marshall Space Flight Center Huntsville, AL 35812

To be submitted for publication in:
Journal of Applied Meteorology
December 12, 2001

Abstract

Information about the vertical microphysical cloud structure is useful in many modeling and predictive practices. Radiometers and radars are used to observe hydrometeor properties. This paper describes an iterative retrieval algorithm that combines the use of airborne active and wideband (10 to 340 GHz) passive observations to estimate the vertical content and particle size distributions of liquid and frozen hydrometeors. The physically-based retrieval algorithm relies on high frequencies ($\geq$ 150 GHz) to provide details on the frozen hydrometeors. Neglecting the high frequencies yielded acceptable estimates of the liquid profiles, but the ice profiles were poorly retrieved. Airborne radar and radiometer observations from the third Convection and Moisture EXperiment (CAMEX-3) were used in the retrieval algorithm as constraints. Nadir profiles were estimated for a minute each of flight time (approximately 12.5 km along track) from an anvil, convection, and quasi-stratiform rain. The complex structure of the frozen hydrometeors required the most iterations for convergence for the anvil cloud type. The wideband observations were found to more than double the estimated frozen hydrometeor content as compared to retrievals using only 90 GHz and below. The convective and quasi-stratiform quickly reached convergence (minimized difference between observations and calculations using the estimated profiles). A qualitative validation using coincident in situ CAMEX-3 observations shows that the retrieved particle size distributions are well corroborated with independent measurements.

1. Introduction

Knowledge of the vertical microphysical cloud structure is important for many aspects of meteorology, such as for determination of precipitation rates, latent heating profiles, and for forecasting hurricane intensity (Simpson et al. 1996). In addition, hydrometeor profiles are used to improve global change models and cloud resolving models. Severe storms or intense rain can also affect earth-satellite communication transmissions. For these reasons, accurate estimates of the vertical profile of liquid and frozen hydrometeor particle size distributions are vital to the atmospheric research, meteorological, and communications communities. In an effort to estimate precipitation profile information despite sparsely-situated ground-based sensors, airborne- and satellite-based remote sensing instruments have been employed (Kummerow et al. 2000).

The challenge of using airborne and/or satellite remote sensors is determining the appropriate instruments for the parameter of interest. Infrared instruments provide temperature and relative humidity profiles in cloud free regions. Lidars remotely sense aerosols, clouds, wind speed and direction, and total precipitable water. However, infrared and lidar instruments cannot be used to reliably obtain detailed precipitating hydrometeor information. A single channel active microwave radar can only provide one of the 2-4 key parameters needed to fully characterize the particle size distribution (PSD) for each of its range gates, but radar reflectivity information can be contaminated by hydrometeor attenuation. A passive multi-frequency microwave radiometer allows probing into the different hydrometeor layers of the clouds and the different channels are sensitive to various hydrometeor types (e.g., liquid versus frozen). The high frequencies ($\geq$ 89 GHz) of the radiometer are more sensitive to frozen hydrometeors, while the low frequencies are mostly

sensitive to liquid hydrometeors. However, radiometers are limited to sensing vertically-integrated information about the hydrometeor structure. In addition, the relationships between hydrometeor characteristics and the upwelling brightness temperatures are both non-linear and non-unique.

By combining active radar and passive radiometers, the opportunities to estimate hydrometeor profiles and cloud characteristics improve (Marzano et al. 1999). In fact the Tropical Rainfall Measuring Mission (TRMM) (Kummerow et al. 2000) was the first satellite to have both a radar and radiometer designed to measure rainfall. Several radar-radiometer retrieval algorithms have been developed for use with the TRMM satellite (e.g., Olson et al. 1996; Sauvageot 1996; Viltard et al. 2000). Prior to TRMM, most existing remote sensing methodologies for estimating cloud structure independently relied on either radiometer or radar observations (e.g., Meneghini et al. 1997).

Associated with TRMM are calibration/validation field campaigns. One such field campaign was the third Convection and Moisture Experiment (CAMEX-3) which was based in south Florida during August and September of 1998 (Geerts et al. 2000). The Texas-Florida Underflights (TEFLUN-B) field campaign combined resources with CAMEX-3, with the purpose of underflying the TRMM satellite. Multiple instruments located on ground, on low and high altitude aircraft, and on satellites were used to observe convective and hurricane systems. Of particular interest for this work are measurements from instruments on the high-altitude ER-2 aircraft that provide a single active channel at 9.6 GHz and 11 brightness temperature channels ranging from 10.7 to 340 GHz. The higher frequency channels are extremely useful for determining and constraining the particle size distributions of the frozen hydrometeors (Deeter and Evans 2000) and provide a unique

aspect to this work in relation to other combined radar-radiometer retrieval algorithms (e.g., Marzano et al. 1999). Two other CAMEX-3 instruments provide data for retrieval result validation.

The retrieval algorithm derived herein minimizes the differences between (active and passive) observations and forward calculations based on the iteratively estimated hydrometeor profiles. The observations are used to constrain the solution. In Section 2, the retrieval algorithm will be detailed. The application of the algorithm to the CAMEX-3 data is described in Section 3, the corresponding retrieval results and validation in Section 4, followed by a summary in Section 5.

2. Retrieval Algorithm

The retrieval algorithm uses both radar and radiometer observations in the retrieval process. The algorithm minimizes the error between observations and calculations based on the iteratively estimated profile. Hydrometeor contents and drop size distributions for rain, cloud water, and frozen hydrometeors are adjusted for each iteration. The flowchart of the algorithm is shown in Fig. 1. The flowchart shows that the radar and radiometer calculations are separate, while the error analysis and profile adjustment scheme are combined. Each of the components in the flowchart are described in detail in this section.

The algorithm is initialized by converting nadir-viewed radar reflectivity profiles into estimates of hydrometeor content profiles. The fine (37.5 m) resolution of the radar range gates is averaged to 0.5 km vertical slabs that extend from 0 to 18 km. The radar-to-microphysical profile algorithm is initialized using preset temperature, pressure, relative humidity, and cloud water profiles taken from hydrologically appropriate Goddard Cumulus

Ensemble (GCE) (Tao and Simpson 1993) profiles. The hydrometeor content profiles from the radar-to-microphysical profile algorithm are partitioned into liquid and frozen particles with Marshall-Palmer (Marshall and Palmer 1948) and Sekhon-Srivastava (Sekhon and Srivastava 1970) exponential drop size distributions, respectively. While continuity of the precipitation flux across the freezing level is not explicitly checked, the masses obtained from the radar reflectivities should have smooth transitions from one level to the next. If necessary, hydrometeors in the cloud profile are extended one additional height level (above, below, or both above and below) the cloud boundaries in order to get non-zero Z calculations at all non-zero observed Z heights. The cloud liquid water, rain, and frozen hydrometeor contents and drop size distributions are then adjusted at each iterative stage of the retrieval algorithm.

2.1 Brightness Temperature Calculations

An efficient radiative transfer (RT) model is required to transform the microphysical information into upwelling passive microwave brightness temperatures (T_B) that are then compared to observations in the iterative retrieval algorithm. The planar-stratified, scattering-based RT model used herein was originally developed by Gasiewski (Gasiewski 1993) and later modified by Skofronick-Jackson and Gasiewski (Skofronick-Jackson and Gasiewski 1995) to allow for five (or more) hydrometeor types (e.g., suspended cloud water, rain, suspended cloud ice, snow and graupel). Flexibility exists in that the user can input the cloud profile and select observation height, viewing angle, frequency (tested from 6 to 425 GHz) and polarization. The RT model requires as input instrument specifications, vertical profiles of temperature, height, relative humidity, and PSD of the hydrometeors in the cloud.

Typically RT models that handle hydrometeor scattering using a perturbation method (Lenoble 1985), as opposed to the adding-doubling method (van de Hulst 1980), as the model used herein does, require more iterations to reach the final brightness temperature value than the adding-doubling method. An analytical approximation was implemented for this retrieval in order to reduce processing time. The RT perturbation technique sums successive orders of scattering:

$$T_B = \sum_{i=0}^{M} \Delta T_B^{(i)} \tag{1}$$

where $\Delta T_B^{(0)}$ is the clear air solution and M is preset during the perturbation radiative transfer modeling. The n to M successive orders of scattering can be written in the form of:

$$\Delta T_B^{(n)} \left(1 + \frac{\Delta T_B^{(n+1)}}{\Delta T_B^{(n)}} + \frac{\Delta T_B^{(n+2)}}{\Delta T_B^{(n+1)}} \frac{\Delta T_B^{(n+1)}}{\Delta T_B^{(n)}} + \ldots + \frac{\Delta T_B^{(M)}}{\Delta T_B^{(M-1)}} \frac{\ldots}{\ldots} \frac{\Delta T_B^{(n+1)}}{\Delta T_B^{(n)}} \right) . \tag{2}$$

If it can be assumed that $\Delta T_B^{(k+1)}/\Delta T_B^{(k)}$ remains fixed for all $k \geq n$ and $M \to \infty$ then an analytical expression for Eq. 2 is:

$$\Delta T_B^{(n)} \frac{1}{1 - W} \tag{3}$$

where

$$W = \frac{\Delta T_B^{(n+1)}}{\Delta T_B^{(n)}} = \frac{T_B^{(n+1)} - T_B^{(n)}}{T_B^{(n)} - T_B^{(n-1)}} . \tag{4}$$

The $T_B^{(k)}$ are the brightness temperature values at perturbation k. This approximation can cut the number of successive orders of scattering by more than 60%.

It is assumed that a planar-stratified model is acceptable in this work because only high-resolution nadir-viewed observations are used in the retrieval and because the observations have fairly small footprints. The calculations assume a nadir-viewed ocean surface at 300 K with a surface windspeed of 10 m/s. Similar to Marzano et al. (1999), the first 500 m above the ocean surface is not adjusted in the retrieval because of difficulties separating surface radar return from the hydrometeors at those levels. Another assumption

is that all particles are spherical in shape and that frozen hydrometeors are solid ice spheres and thus will not need dielectric mixing approximations to compute the absorption and scattering coefficients. At high frequencies ($\geq$ 150 GHz) dielectric mixing theories begin to breakdown because the particle inclusion size becomes electrically large with respect to the wavelength (Sihvola 1989).

2.2 Radar Reflectivity Calculations

The radar reflectivity (Z) calculations are based on a model described by Jones et al. (1997). This code is also flexible because the user can specify instrument viewing angle, height, range gate intervals, etc. The radar model described in Jones et al. (1997) relies on GCE data for input and models reflectivities as would be seen from the Precipitation Radar on the Tropical Rainfall Measuring Mission (TRMM) satellite (Simpson et al. 1996). For this work, the radar code has been revised to simulate the ER-2 Doppler Radar (EDOP) instrument Heymsfield et al. (1996). The model described in Jones et al. (1997) automatically generates a melting layer; in this work the retrievals rely solely on the hydrometeor parameterization as iteratively generated by the retrieval. Using the size distributions, the reflectivity and attenuation can be computed at each range gate. The backscattering cross section used in obtaining the reflectivity is computed using Mie theory. By integrating the reflectivity over a simulated radar beam that models the observation radar specifications, the return power can be calculated and compared to the observed data.

2.3 Error Analysis

Once the T_B and Z have been computed for the current estimated profile, the

error analysis occurs. There are two convergence criteria. One for the T_B and one for the Z:

$$\max(|T_{Bobs}(i) - T_{Bcalc}(i)|) < S_{T_B} \text{ for all } i \text{ frequencies} \tag{5}$$

$$\max(|Z_{obs}(j) - Z_{calc}(j)|) < S_Z \text{ for all } j \text{ range gates.} \tag{6}$$

The S_{T_B} and S_Z are convergence thresholds and are currently set to 10 K and 2.5 dBZ. Two convergence criteria are needed so that the brightness temperature and reflectivity errors can be independently analyzed to determine the drop size distribution adjustment needed to reduce any errors.

2.4 Hydrometeor Adjustment Algorithm

The hydrometeor adjustment algorithm is outlined in Fig. 2. The algorithm first checks to see if the radar convergence criterion is met. If not the particle size distributions are adjusted at the height h_m of the maximum error in the Z profile. The adjustment factor Y is related to the ratio $(Z_{obs}(h_m)/Z_{calc}(h_m))$. The Z-based adjustments are

$$\Lambda = \Lambda^{old}/Y \text{ and } N_0 = N_0^{old}/Y^3 \tag{7}$$

in the exponential PSD equation

$$N(D) = N_0 e^{-\Lambda D} \ (\mathrm{mm}^{-1}\mathrm{m}^{-3}) \tag{8}$$

where D, Λ^{-1} are in mm and N_0 is in $\mathrm{mm}^{-1}\mathrm{m}^{-3}$. This application of Y preserves the T_B values so that they do not change much for Z-based adjustments. The starting N_0 and Λ are provided during the initialization procedure previously described.

When the convergence criterion for the T_B is not met, a similar adjustment is made to reduce the differences in the observed and calculated T_B values. Frequencies where the

temperature difference exceeds 10 K are used to determine where to adjust the hydrometeor profile. Each frequency has a weighting function that peaks at a height dependent on temperature and hydrometeor characteristics. The hydrometeor profile is adjusted at the height(s) and ±500 m of where the weighting function(s) peaks for the frequency(ies) with error exceeding 10 K. If the radiometer frequencies are less than 89 GHz, the rain and cloud water drop sizes are adjusted; if above 89 GHz the frozen hydrometeor particle sizes are adjusted. For the 183.3 GHz channels, only the 183.3±1 GHz channel is used to adjust rain and cloud water drop sizes. Errors in the 89, 183.3±3 and 183.3±7 GHz channels are usually corrected through PSD adjustments due to errors in other channels.

If the weighting function peak does not fall within the cloud boundaries, the particle size adjustments are made to the lower, middle, and upper third of the cloud volume based on the frequency. For 37 and 150 GHz, particle sizes within the lower third of the cloud liquid and frozen hydrometeor layers (respectively) are adjusted. For 183.3±1 and 220 GHz, the particle sizes within the middle third of the cloud liquid and frozen hydrometeors (respectively) are adjusted. Finally for 340 GHz, the particle sizes in the upper third of the frozen hydrometeor layers in the cloud are adjusted.

The adjustment parameters are a function of the ratio $(T_{Bobs}(k)/T_{Bcalc}(k))$ denoted by X where k is the index of the frequency at which an error occurs. The T_B-based adjustments are

$$\Lambda = \Lambda^{old}/X \text{ and } N_0 = N_0^{old}/X^7 \tag{9}$$

in the exponential particle size distribution (PSD) equation (8). This application of X preserves the Z values because Z is proportional to $D^7 N_0$ ($Z \propto \int D^6 N(D) dD$).

The adjustments to the size distributions of a specific height level and hydrometeor

type are only changed once per iteration. This eliminates the scenario where one adjustment for a frequency or range gate would cancel out the adjustment for a different frequency. Also the adjustments do not preserve the (bulk) density of the hydrometeors because the bulk density M is proportional to $D^4 N_0$. While we have been able to meet our convergence criteria for anvil, convective, and stratiform cloud cases, it is likely that further improvements to the adjustment algorithm will allow us to tighten the convergence criteria thresholds. Suggested improvements will be discussed in the Summary section.

3. Application to CAMEX-3 Data

Observations from CAMEX-3/TEFLUN-B (Geerts et al. 2000) are used in the retrieval algorithm. While CAMEX-3 had broad-based instrumentation on multiple platforms including aircraft, ground, ship, and satellite, this work focuses on the data from four instruments on the ER-2 aircraft and one instrument on the DC-8 aircraft. On board the ER-2, flying at an altitude of 20 km, the instruments of interest for this work are the Millimeter-wave Imaging Radiometer (MIR) Racette et al. (1996), the Advanced Microwave Precipitation Radiometer (AMPR) Spencer et al. (1994), the ER-2 Doppler Radar (EDOP) Heymsfield et al. (1996) and the National Polar-orbiting Operational Environmental Satellite System (NPOESS) Aircraft Sounder Testbed - Microwave (NAST-M) (Blackwell et al. 2001). These ER-2 instruments measure atmospheric hydrometeors in the microwave region of the electromagnetic spectrum. The MIR observes at 89, 150, 183.3±1, ±3, ±7, 220, and 340 GHz, while the AMPR observes at 10.7, 19.35, 37, and 85.5 GHz. The EDOP is an active radar sampling at 9.6 GHz with a range gate interval of 37 meters. The NAST-M, used only for validation purposes, is a passive microwave spectrometer with 17 channels near the oxygen absorption lines at 50-57 GHz and

118.75 GHz. The NAST-M channels are independent of any channels used in the retrieval. On the DC-8 aircraft flying at 12 km altitude, there is the Particle Measuring System, Inc. (PMS) 2DC probe as part of the Cloud and Aerosol Particle Characterization (CAPAC) suite of instruments. The PMS 2DC probe provides in situ observations of particle size distributions used to validate the retrieved size distributions.

For this work, only the nadir or near-nadir signatures are used. The data sets from the MIR, AMPR, and EDOP have been analyzed and colocated. In an effort to match each radiometer channel and the corresponding EDOP radar samples to similar volumes of the storm, all data values were simulated to match the lowest resolution channel of all the instruments. The largest footprint of 2.8 km occurs for the AMPR 10 and 19 GHz channels at nadir when the ER-2 is flying at 20 km altitude. Because there is not an AMPR pixel directly at nadir, for the 10 and 19 GHz channels the two pixels adjacent to nadir were averaged in an effort to simulate a nadir value. In order to transform the MIR, EDOP and the higher frequency AMPR data to the lowest resolution, a two-dimensional Gaussian-weighted mean for each set of data values was calculated where the weights are 1.0 at the center and 0.5 at 1.4 km away from the center. Additionally, since the EDOP radar does not sample off nadir, it probably misses some of the volume sample that the radiometers observe. The EDOP has a 3^{o} beam width so it is seeing about 0.6 km off nadir in both directions at the surface instead of the 1.4 km off nadir view of the AMPR 10 and 19 GHz channels.

While checking the quality of the match between the instruments an offset between the AMPR 85 GHz channel and the MIR 89 GHz channel was observed. Even though the quantitative values of the brightness temperatures of these two channels are not expected to

match exactly, it is reasonable to assume that the time series of the brightness temperature trend for the two channels should be similar. It was determined that the value of the offset in time was dependent upon ER-2 altitude and airspeed; therefore, a pointing angle difference was hypothesized as the cause of the error. This pointing angle difference was consistently determined as 3.3 degrees when using three separate sets of field campaign data for MIR and AMPR from the 1998 (CAMEX-3) and 1999 (TRMM Large Scale Biosphere-Atmosphere Experiment in Amazonia (LBA)) time period. The cause of this error is likely related to slight differences in the orientation of instruments within the ER-2 aircraft. The correlation of the time series of the EDOP and AMPR data was determined to be acceptable so no correction was applied to these data; MIR data was corrected using the pointing angle difference along with the ER-2 altitude and airspeed values.

Figure 3 shows the colocated observed data for Hurricane Bonnie on 26 August 1998, including EDOP data (upper panel), MIR brightness temperatures (center panel), and AMPR brightness temperatures (lower panel). For this image, the ER-2 is flying west to east at approximately 32.8° N latitude. The left side of the image corresponds to the outer edge of Hurricane Bonnie and the plane flies toward the eye, which is on the right side of the image, crossing several rainbands. There are at least three distinct cloud types in Figure 3: an anvil cloud region to the left of the image (14:04:00 UTC to about 14:07:30 UTC) with a high altitude EDOP reflectivity profile and low brightness temperature values for the MIR frequencies (indicating cooling from ice scattering). There is a weak outer eyewall embedded convective core from about 14:11:00 UTC to about 14:13:30 UTC and a quasi-stratiform cloud region from about 14:15:20 UTC to about 14:17:00 UTC.

The retrieval algorithm focuses on small regions within these three storm types.

The selected times span from 14:05:04 — 14:06:05 UTC, 14:12:07 — 14:13:41 UTC, and 14:15:40 — 14:16:38 UTC for the anvil, convective and quasi-stratiform regions respectively. The temporal sampling of the colocated data set is about 3 seconds and has a footprint size of 2.8 km at the ER-2 altitude of 20 km. However, since the observations are oversampled, the retrieved profiles are between 12.5 and 18.7 km along-track of the flight line, for a total of $\sim$ 44 km. An analysis of the complete data set as shown in Fig. 3 is computationally prohibitive at this time and would require additional adjustments to the size distribution adjustment algorithm for the transitioning cloud type regions.

4. Retrieval Results

The iterative retrieval algorithm was used to estimate the vertical hydrometeor profiles of the three storm types found within Hurricane Bonnie's outer rainbands. The retrieval performed well, producing extremely good matches between the observed Z and calculated Z (see Fig. 4ab). The brightness temperature matches were less than the maximum threshold of 10 K for nearly all of the cases (see Fig. 5). The average number of iterations required for estimating one profile was 36 with the anvil retrievals requiring more iterations than the average number to converge and the quasi-stratiform case requiring fewer than the average number of iterations to converge. In general it was easiest to reach convergence for the radar reflectivity stopping criterion and more difficult for the high frequencies of the radiometer. This is reasonable because the initial estimated profiles were obtained by transforming the EDOP reflectivities to hydrometeor content profiles. Additionally, the high frequency radiometer channels are quite sensitive to the frozen hydrometeor size distributions, which are not well known, and therefore make it difficult to ascertain the proper sizes to obtain a good match between the high frequency

observations and calculations. Finally, it must be stated that some of the retrieved profiles are not unique solutions for the observed data. In particular, the anvil cases had 2 or more slightly different PSD profiles which still met the convergence criteria (see Fig. 6a). It is assumed that if the convergence criteria were even more restrictive that the differences in the retrieved profiles would decrease. Even though the retrievals may not be unique, they still provide good approximations to the actual cloud structure and hydrometeor size distributions.

4.1 Anvil Results

For the anvil case (14:05:04 — 14:06:05 UTC), output from the estimated profiles are shown in Figs. 4c-f (left hand side of each image). Figs. 4c, e show the liquid and frozen hydrometeor contents while Figs. 4d, f show the liquid and frozen (melted) hydrometeor median diameter ($D_0 = 3.67/\Lambda$ from Eq. 8). The algorithm also produces the number density (N_0 from Eq. 8) but this value is not plotted because it can be extracted using the content M and Eq. 8 in

$$M = \int_0^\infty N(D)\frac{\pi D^3}{6}\rho dD \tag{10}$$

where $\rho = 1.0$ g cm^{-3} for rain and 0.913 g cm^{-3} for the frozen hydrometeors.

From Fig. 4e, notice that the frozen hydrometeor content is large across the whole anvil region. The variability can be attributed to the difficulties in reaching convergence for the anvil region profiles. In the anvil region, the median diameter of the liquid and frozen (melted diameter) particles does not exceed 0.16 mm and 0.56 mm, respectively. The average (over all heights and UTC times in the anvil cloud) melted median diameter is 0.077 mm. The radar and radiometer calculations extend the exponential drop size distribution to approximately 2.7 times these median diameters.

Fig. 5 shows the differences in calculated and observed T_B. As can be seen from Fig. 5 (left hand side), the differences for the 37 and 340 GHz brightness temperatures bound the convergence criterion space. The average number of iterations required for estimating an anvil profile is 78. The required number of iterations is higher than the other cases because of the difficulty in determining appropriate characteristics for the frozen hydrometeors. In addition, the assumption of solid ice spheres here rather than specific crystalline shapes or fluffy snow may increase convergence time.

In the anvil region, there is a negative bias where the calculations are too cool for the low frequencies and a positive bias for the highest frequencies. It is possible that the contents of the monodisperse cloud water and cloud ice initialized by the GCE model are not properly estimated. (Note that cloud water content, but not cloud ice content, is adjusted in the retrieval.) Quick tests using cloud water and cloud ice from other cloud models do not improve the retrieval results significantly. Modifying the retrieval algorithm to adjust the cloud water and cloud ice presents several difficulties: (1) the radar data is not sensitive to cloud water and cloud ice, (2) cloud water and cloud ice may extend beyond the boundaries of the radar returns strong enough to indicate the presence of clouds, and (3) how should cloud water and cloud ice be modeled: monodisperse or polydisperse. The negative/positive bias may also be caused by inadequate modeling of the ocean surface and/or lower altitudes. The calculated high frequency radiometer data is relatively warm with respect to the observations because if additional ice is introduced it over cools the 37 GHz channel.

Figure 6a shows that the profile retrievals may not be unique. This figure shows the retrieved profile for 14:05:04 UTC for three different size distribution adjustment

algorithms (modifications to Fig. 2). Algorithm 1 is used for the reported results in this paper. All three algorithms met the convergence criteria; however, algorithm 2 tended to put more ice at upper altitudes and less at lower altitudes. Although it is not shown, the retrieved profiles for the three algorithms are more similar for thicker anvil, convective, and stratiform clouds. Although the profiles are different, the columnar ice masses among the three algorithms are within 100.0 g/m^2 of each other.

For anvil clouds the necessity of using the high frequency channels to determine frozen hydrometeor characteristics is shown in Fig. 6b. This figure shows what happens when the retrieval algorithm does not utilize (i.e. correct for errors in) the high frequency channels. For the single profile at 14:05:07 UTC, the solid line in Fig. 6b shows the results using all channels and the reflectivities. For this figure, the solid line is considered the truth. The dotted line shows the retrievals using only frequencies less than and equal to 150 GHz. The dashed line shows the results when using only frequencies less than or equal to 89 GHz. For the low frequency case (dashed line) the calculated T_B for the 340 GHz channels are 60-70 Kelvin warmer than the observations. Clearly much information about frozen hydrometeor content cannot be derived when only the low frequency channels are used.

4.2 Convective Results

The convective profiles (14:12:07 — 14:13:41 UTC) on the average required fewer iterations (25). This is due to the underlying rain profile stabilizing the low frequency radiometer data and reducing the impact of the ocean surface conditions. Figures 4 and 5 (center region) show the retrieved content, median diameter, and T_B differences. Figure 4 indicates liquid and frozen contents similar to what would be expected for the EDOP profile

(Fig. 4a). The maximum median drop diameter for rain (over all non-zero retrieved rain pixels) is 0.58 mm; for the frozen hydrometeors the maximum melted median drop diameter is 1.1 mm. It is encouraging that the frozen hydrometeors (Fig. 4e, f center convective region) follow the pattern seen in the reflectivity observations.

The T_B differences in Fig. 5 show some interesting trends. First, the left hand side of the convective region shows a similar bias as seen within the anvil region where the low frequency calculations underestimate and the high frequency calculations overestimate the actual T_B values. This issue is further compounded because the retrieval algorithm does not adjust the hydrometeors in the region between the Earth's surface and 500 m up because it is difficult to separate surface radar return from hydrometeors at those levels. Second, the 19 and 37 GHz calculations become warmer than the observations to the left of the convective region where the heavy rain region is dissipating somewhat. At the same time and in the same region, the high frequency T_B differences are converging toward zero. This change of T_B differences is likely due to decreasing hydrometeor complexity from left to right in the convective region. The decreasing complexity may mean that the solid ice spherical particles are adequate and this causes the high frequency T_B differences to be reduced on the left hand side of the image. Notice that at 14:12:38 UTC the 220 GHz difference did not converge to less than 10 K, instead it converged to 10.4 K. In addition the 183.3±1.0 GHz channel differences are 10.2 K at 14:13:20 and 14:13:23 UTC.

4.3 Quasi-Stratiform Results

The quasi-stratiform results are quite surprising considering that no melting layer is modeled in the RT calculations or estimated profiles and yet the retrieval reached the convergence criteria in only an average of 9 iterations. There are two reasons for the quick

convergence: (1) a uniform cloud structure and (2) the initialization procedure did a good job estimating liquid and the few frozen hydrometeor levels of this storm, indicating that the Marshall and Palmer (1948) PSD is reasonably appropriate for this quasi-stratiform cloud. Once again content and median diameter profiles are shown in Fig. 4 (right hand side) and T_B differences are shown in Fig. 5. The maximum median diameter is 0.39 mm and 1.03 mm for liquid and frozen hydrometeors (melted) respectively.

The frozen hydrometeor content of the quasi-stratiform region shown in Fig. 4 follows the EDOP reflectivity profile (e.g., more ice on the left hand side of the quasi-stratiform region and a peak diameter band at the melting layer height). Note that the bright band height increases toward the right as we move toward the hurricane eye. This is typical since the temperatures are warmer in the eye. The T_B differences are revealing: there is a trend of improved comparisons between observed and calculated values near the center of the quasi-stratiform time segment (14:15:40 — 14:16:38 UTC). At the fringes of the time segment there is a steep decrease of rain and/or frozen hydrometeors as shown in the EDOP image. Within these highly variable regions it is more difficult to match the observed and calculated T_B.

4.4 Validation of Retrieval Results

Since the true microphysical profile cannot be measured at the spatial and temporal scales appropriate for the nadir-viewed ER-2 aircraft brightness temperature observations, qualitative verification of the retrieved profiles will have to suffice. Two different sources of CAMEX-3 coincident information are used to validate the results: (1) the passive brightness temperature oxygen band channels on the NAST-M (Blackwell et al. 2001) and (2) in situ observations at $\sim$ 12 km from the DC-8 aircraft CAPAC 2DC

PMS probe.

First the 50.3±0.09 and 118.75±3.5 GHz NAST-M channels were compared to calculations at those same frequencies using the retrieved profiles. These two channels represent the NAST-M channels furthest away from the oxygen line centers and thus more sensitive to the hydrometeors in addition to the oxygen. The NAST-M instrument is onboard the ER-2 sampling the same (nadir-viewed) scene as the EDOP, MIR, AMPR. Since the NAST-M channels were not resampled to the grid of the combined EDOP-MIR-AMPR observations, there were fewer overlapping samples. Each of the calculated T_B values using the retrieved profile for these overlapping UTC times was less than 10 K different from the NAST-M values. This means that the retrieved profiles are consistent (in terms of the convergence criteria) with T_B values of the outermost wings of these oxygen bands.

The second validating data set is from the CAPAC suite of in situ microphysical measurement instruments observing from the DC-8 aircraft during CAMEX-3; the PMS 2DC probe was the primary instrument of interest here. The DC-8 flies at a height of about 12 km (8 km below the ER-2) and for this UTC segment was well correlated with the ER-2 flight path. Since 12 km is above the cloud tops of the convective and stratiform regions retrieved herein, the 2DC microphysics data can only be used to validate anvil ice characteristics. The 2DC probe images particles within its field of view and then processing produces the number of particles in specified bin sizes within a centimeter-cubed volume of air. To compare these measurements with the retrieved exponential PSDs, the number of particles in the centimeter-cubed volume were divided by the interval size of the diameter bin sizes. This provides a numbers considered equivalent to $N(D)$ for each of the diameter bin sizes. The retrieved N_0 were multiplied by e^{-1} to provide a value of $N(D)$ at $D = D_0$.

Only the retrieved values near the 12 km height level were used. Figure 7 shows the comparison of PMS 2DC data for 14:00 to 14:06 UTC (the DC-8 was underflying the ER-2 for these UTC times) to the retrieved anvil ice at 11.5 to 12.5 km. This figure shows that the retrieved values (symbols for each height) are very similar to the PMS 2DC data (lines for each UTC time). This qualitative validation indicates that the anvil ice retrievals are close to the in situ observations.

5. Summary

This paper has provided estimates of precipitation profiles and frozen hydrometeor profiles when retrieving using wideband radiometer observations plus radar observations. Profiles of hydrometeor characteristics were estimated using an iterative retrieval algorithm. The algorithm minimized the differences between forward calculations and observed radar and radiometer observations from the ER-2 aircraft obtained during CAMEX-3. The advantages of this retrieval algorithm are (1) the use of high frequency channels to provide details of the frozen hydrometeors and (2) combining radar and radiometer observations.

Contents and particle size distributions for spherical rain, cloud water, and frozen hydrometeors were estimated for profiles extending to 18 km with vertical spacing of 0.5km. The retrieval was performed on anvil, convective, and quasi-stratiform cloud types. The anvil cloud type required the most iterations in order to resolve the unknowns related to the characteristics of the frozen hydrometeors. The quasi-stratiform region met the convergence criterion the quickest because the initialization procedure used drop sizes more applicable to stratiform cloud types.

The retrieval results were qualitatively validated using observations from the

NAST-M on the ER-2 and the CAPAC 2DC probe on the DC-8 aircraft. The brightness temperatures of the outermost wings of the 50-60, and 118 GHz oxygen bands as measured by the NAST-M, were within the convergence criteria (less than 10 Kelvin from the calculated brightness temperature values). Likewise, observations from the PMS 2DC probe on the DC-8 aircraft flying at 12 km above the Earth's surface were used to validate the particle size distributions of the anvil region retrievals. The retrieved anvil particle sizes and number densities matched the measured 2DC probe microphysics well. Unfortunately the DC-8 was above the cloud tops for the convective and quasi-stratiform regions and no validation using the PMS 2DC data could be performed for them.

The retrieved profiles contain considerable information about the cloud structure and hydrometeor size distributions even though they may not have unique solutions. The retrieved profiles are important for improving global change models and cloud resolving models. Furthermore this work shows that high frequency microwave channels ($\geq$ 150 GHz) information needed in order to define the frozen hydrometeor characteristics found at the upper altitude levels of a cloud.

Acknowledgments-This work has been supported by Ramesh Kakar through the NASA Tropical Rainfall Measuring Mission (NAG5-7777, NAG5-10347). The authors thank Phil Rosenkranz for the NAST-M data. We thank Rudolf Pueschel and Anthony Strawa and Robert Black for the CAPAC PMS 2DC probe data which was obtained from http://ghrc.nsstc.nasa.gov/camex3/qlook.html. We also thank the Global Hydrology Resource Center and NASA Earth Sciences Enterprise/Atmospheric Dynamics Program for all of the CAMEX-3 data.

)References

Blackwell, W. J., J. W. Barrett, F. W. Chen, R. V. Leslie, P. W. Rosenkranz, M. J. Schwartz and D. H. Staelin, 2001: Npoess aircraft sounder testbed-microwave (NAST-M): Instrument description and initial flight results. *IEEE Trans. Geosci. Remote Sens.*, **39**, 2444–2453.

Deeter, M. N. and K. F. Evans, 2000: A novel ice-cloud retrieval algorithm based on the millimeter-wave imaging radiometer (MIR) 150- and 220-GHz channels. *J. Appl. Meteor.*, **39**, 623–633.

Gasiewski, A. J., 1993: Microwave radiative transfer in hydrometeors. in M. A. Janssen, editor, *Atmospheric Remote Sensing by Microwave Radiometry*, pp. 91–144. John Wiley and Sons, New York.

Geerts, B., G. M. Heymsfield, L. Tian, J. B. Halverson, A. Guillory and M. I. Mejia, 2000: Hurricane Georges's landfall in the Dominican Republic: Detailed airborne doppler radar imagery. *Bull. Amer. Meteor. Soc.*, **81**(5), 999–1018.

Heymsfield, G. M., I. J. Caylor, J. M. Shepherd, W. S. Olson, S. W. Bidwell, W. C. Boncyk and S. Ameen, 1996: Structure of Florida thunderstorms using high-altitude aircraft radiometer and radar observations. *J. Appl. Meteor.*, **35**, 1736–1762.

Jones, J. A., R. Meneghini, T. Iguchi and W.-K. Tao, 1997: Synthetic data for testing TRMM radar algorithms. in *Proceedings of the 28th Conference on Radar Meteorology*, pp. 196–197, Austin, TX.

Kummerow, C., J. Simpson, O. Thiele, W. Barnes et al., 2000: The status of the tropical rainfall measuring mission (TRMM) after two years in orbit. *J. Appl. Meteor.*, **39**, 1965–1982.

Lenoble, J., 1985: *Radiative Transfer in Scattering and Absorbing Atmospheres: Standard Computational Procedures.* A. Deepak Publishing Co., Hampton, VA.

Marshall, J. S. and W. M. Palmer, 1948: The distribution of raindrops with size. *J. Meteor.*, **5**, 165–166.

Marzano, F. S., A. Mugnai, G. Panegrossi, N. Pierdicca, E. A. Smith and J. Turk, 1999: Bayesian estimation of precipitating cloud parameters from combined measurements of spaceborne microwave radiometer and radar. *IEEE Trans. Geosci. Remote Sens.*, **37**, 596–613.

Meneghini, R., H. Kumagai, J. R. Wang, T. Iguchi, and T. Kozu, 1997: Microphysical retrievals over stratiform rain using measurements from an airborne dual-wavelength radar-radiometer. *IEEE Trans. Geosci. Remote Sens.*, **35**, 487–506.

Olson, W. S., C. D. Kummerow, G. M. Heymsfield and L. Giglio, 1996: A method for combined passive-active microwave retrievals of cloud and precipitation profiles. *J. Appl. Meteor.*, **35**, 1763–1789.

Racette, P., R. F. Adler, J. R. Wang, A. J. Gasiewski, D. M. Jackson and D. S. Zacharias, 1996: An airborne millimeter-wave imaging radiometer for cloud, precipitation and atmospheric water vapor studies. *J. Atmos. Oceanic Technol.*, **13**, 610–619.

Sauvageot, H., 1996: Retrieval of vertical profiles of liquid water and ice content in mixed clouds from doppler radar and radiometer measurements. *J. Appl. Meteor.*, **35**, 14–23.

Sekhon, R. S. and R. Srivastava, 1970: Snow size spectra and radar reflectivity. *J. Atmos. Sci.*, **27**, 299–307.

Sihvola, A. H., 1989: Self-consistency aspects of dielectric mixing theories. *IEEE Trans. Geosci. Remote Sens.*, **27**, 403–415.

Simpson, J., C. Kummerow, W.-K. Tao and R. F. Adler, 1996: On the tropical rainfall measuring mission (TRMM). *Meteor. Atmos. Phys.*, **60**, 19–36.

Skofronick-Jackson, G. M. and A. J. Gasiewski, 1995: Nonlinear statistical retrievals of ice content and rain rate from passive microwave observations of a simulated convective storm. *IEEE Trans. Geosci. Remote Sens.*, **33**(4), 957–970.

Spencer, R. W., R. E. Hood, F. J. LaFontaine, E. A. Smith, R. Platt, J. Galliano, V. L. Griffin and E. Lobl, 1994: High-resolution imaging of rain systems with the advanced microwave precipitation radiometer. *J. Atmos. Oceanic Technol.*, **11**, 849–857.

Tao, W.-K. and J. Simpson, 1993: Goddard cumulus ensemble model. Part I: Model description. *Terrestrial, Atmos. and Oceanic Sciences*, **4**, 35–72.

van de Hulst, H. C., 1980: *Multiple Light Scattering Tables and Formulas, and Applications: Volume 2.* Academic Press, New York.

Viltard, N., C. Kummerow, W. S. Olson and Y. Hong, 2000: Combined use of the radar and radiometer of TRMM to estimate the influence of drop size distribution on rain retrievals. *J. Appl. Meteor.*, **39**, 2103–2114.

Figure 1: The retrieval algorithm flowchart.

Figure 2: The size distribution adjustment flowchart.

Figure 3: The EDOP radar reflectivity (upper panel), the MIR brightness temperatures (center two panels) and the AMPR brightness temperatures (lower panel).

Figure 4: The (a) EDOP radar reflectivity, (b) calculated reflectivity for the retrieved profile, (c) retrieved liquid water content, (d) retrieved rain median diameter, (e) retrieved frozen content, and (e) retrieved frozen hydrometeor median melted diameter.

Figure 5: The calculated minus observed brightness temperature differences for low frequencies (upper panel), high frequencies (middle panel), and 183.3 GHz channels (lower panel).

Figure 6: Single profile retrieval results for (a) different hydrometeor adjustment retrieval algorithms and (b) for a reduced microwave channel set.

Figure 7: CAPAC PMS 2DC in situ observations from the DC-8 at 12 km altitude for 14:00 — 14:06 UTC (lines) and retrieved anvil $N(D)$ for $D = D_0$ at 11.5 km (diamonds), 12.0 km (triangles), and 12.5 km (squares).

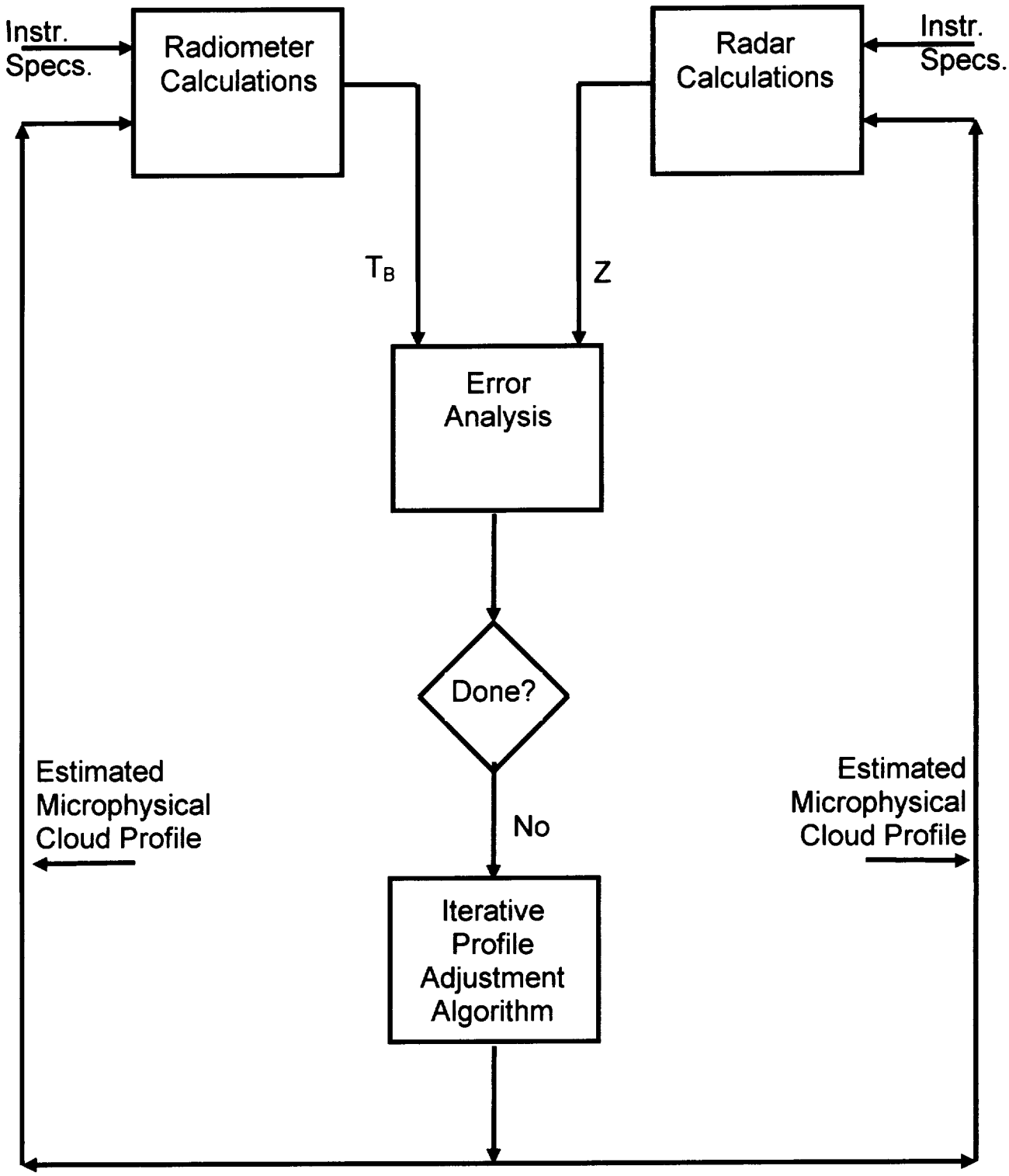

Figure 1: The retrieval algorithm flowchart.

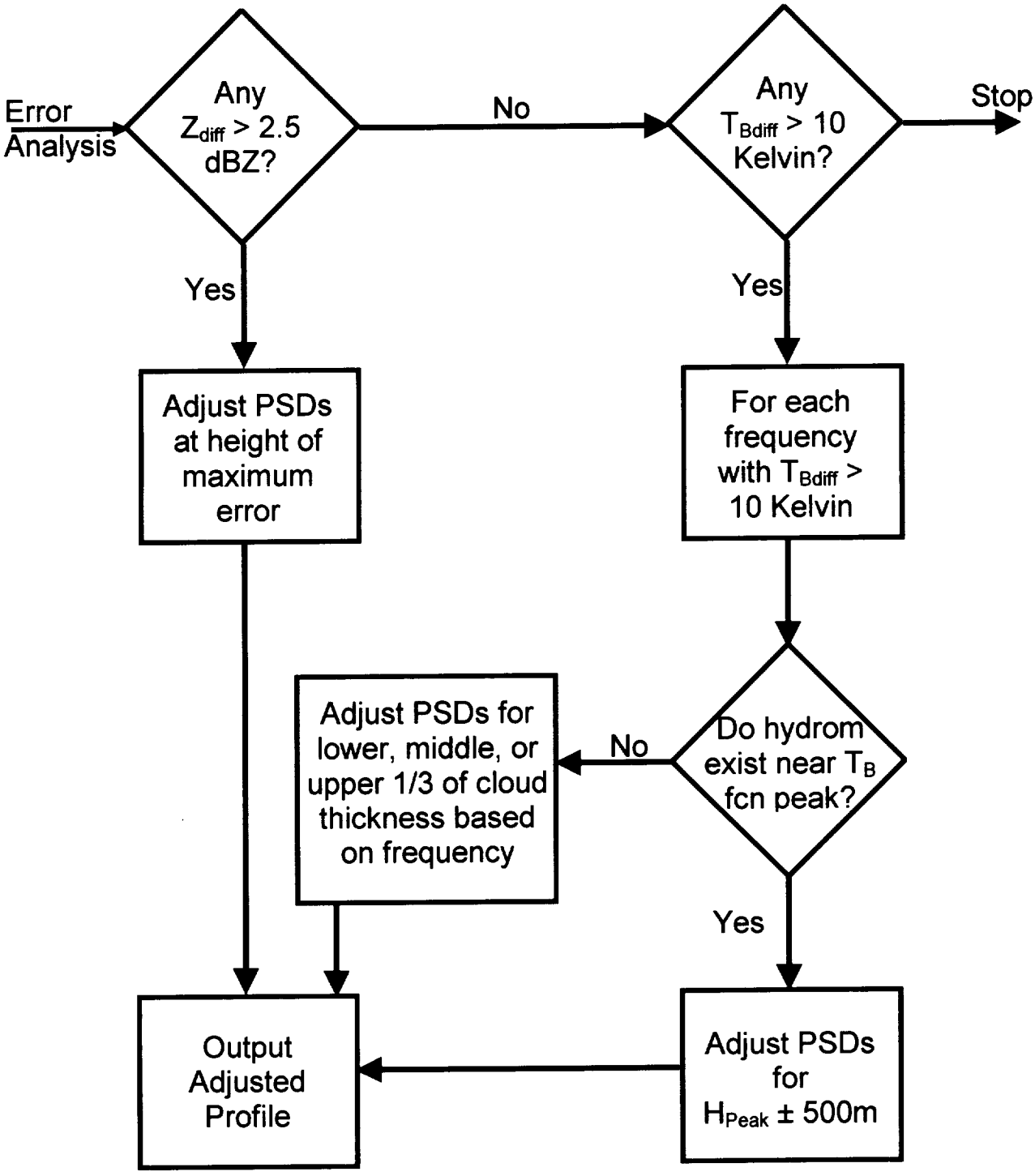

Figure 2: The size distribution adjustment flowchart.

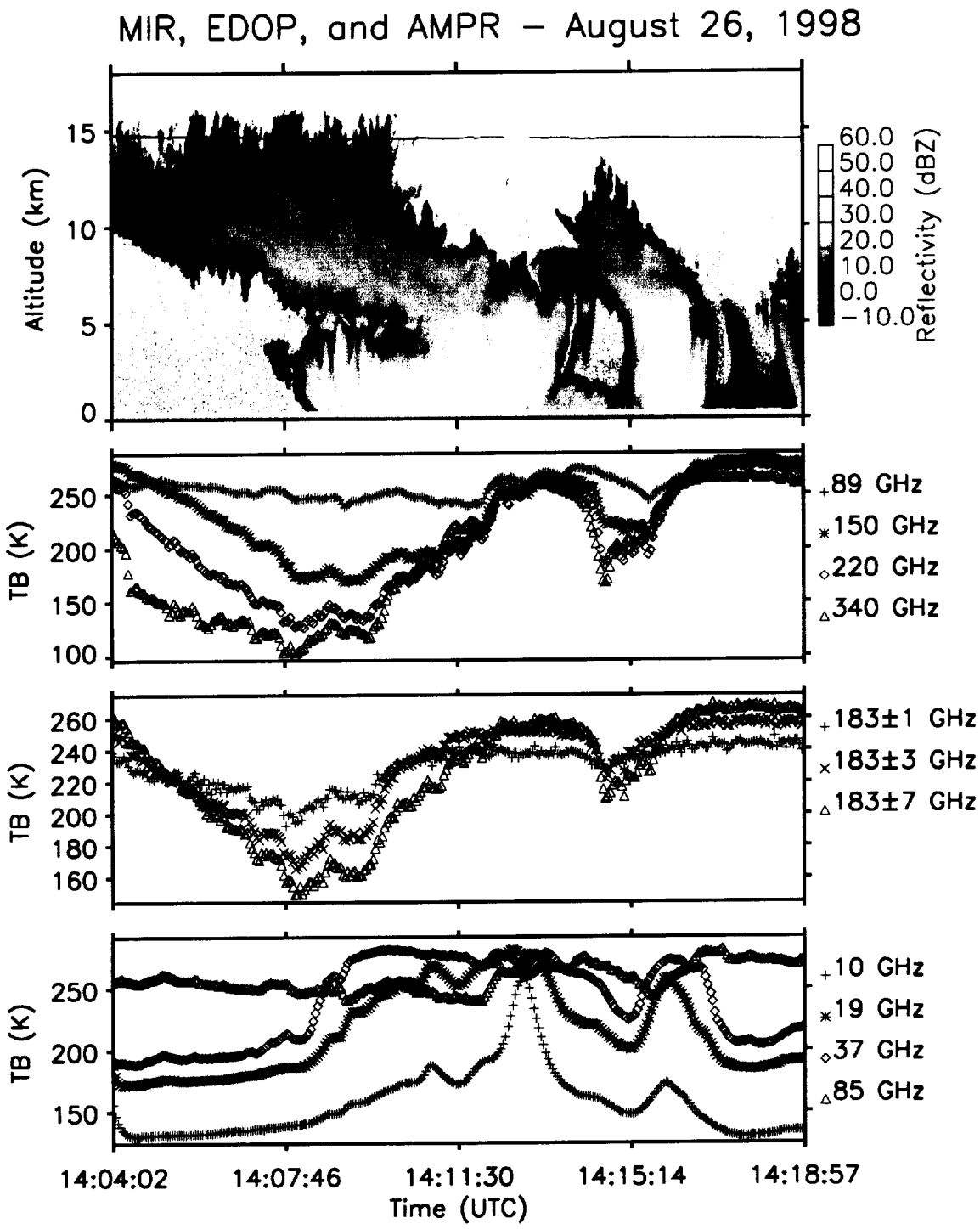

Figure 3: The EDOP radar reflectivity (upper panel), the MIR brightness temperatures (center two panels) and the AMPR brightness temperatures(lower panel).

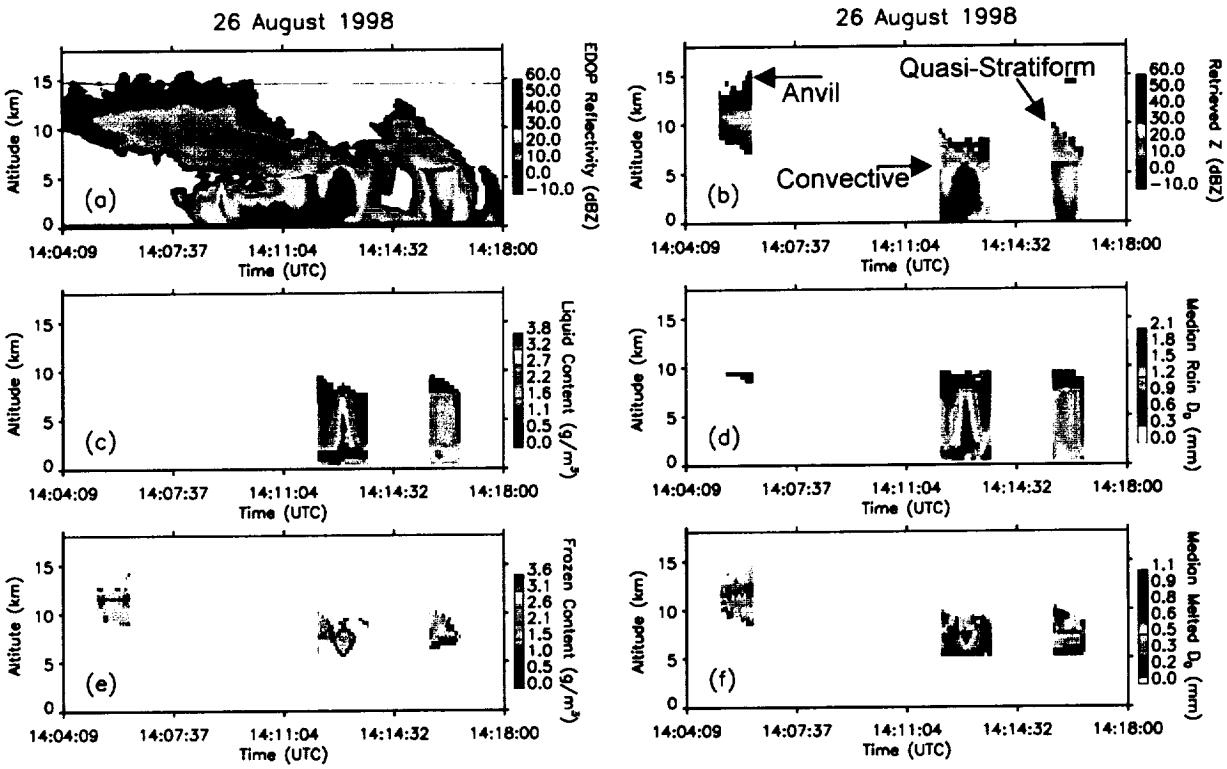

Figure 4: The (a) EDOP radar reflectivity, (b) calculated reflectivity for the retrieved profile, (c) retrieved liquid water content, (d) retrieved rain median diameter, (e) retrieved frozen content, and (e) retrieved frozen hydrometeor median melted diameter.

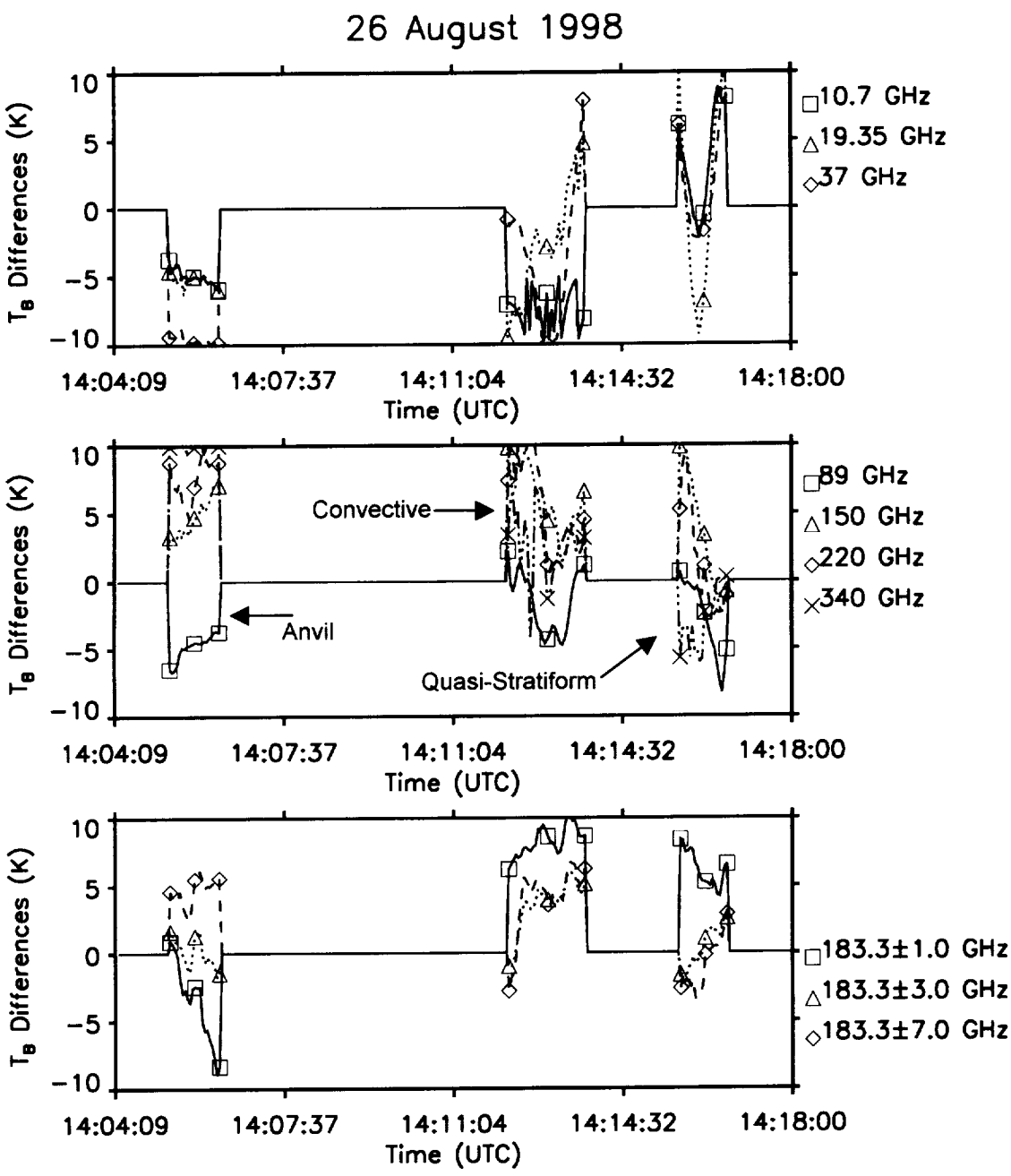

Figure 5: The calculated minus observed brightness temperature differences for low frequencies (upper panel), high frequencies (middle panel), and 183.3 GHz channels (lower panel).

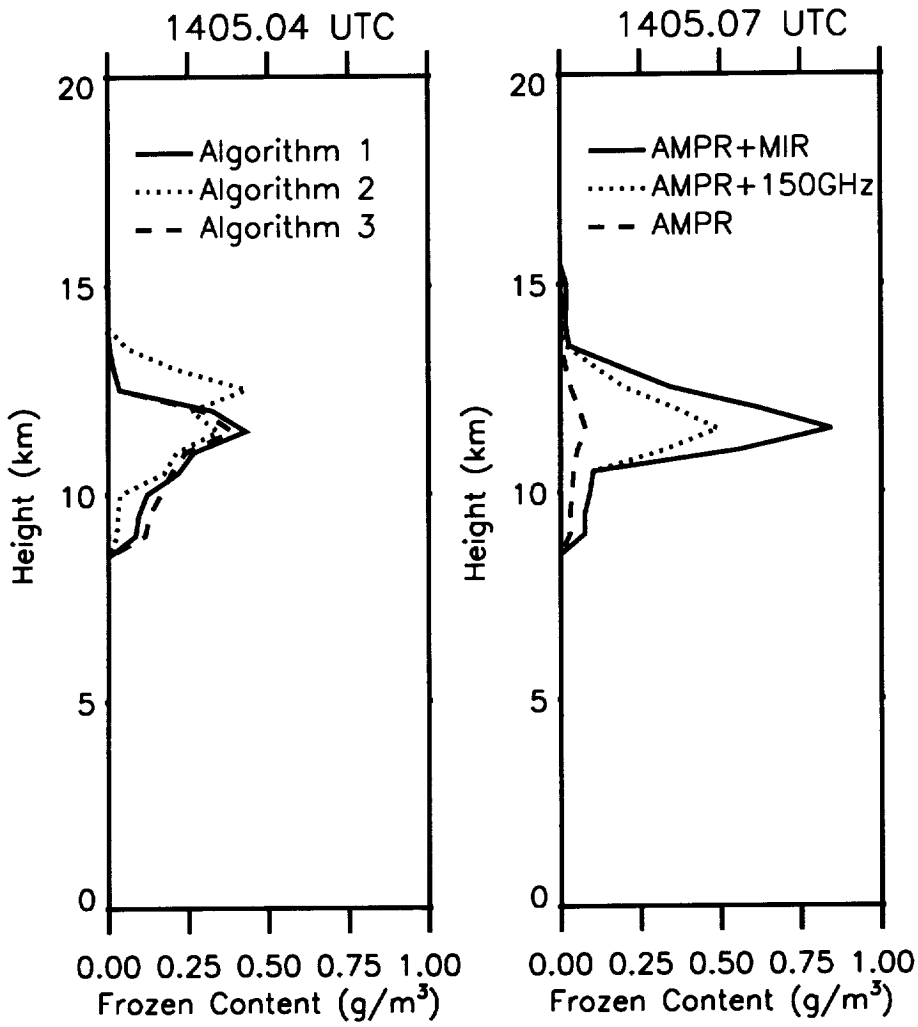

Figure 6: Single profile results (a) for three different hydrometeor adjustment retrieval algorithms and (b) for three microwave channel sets.

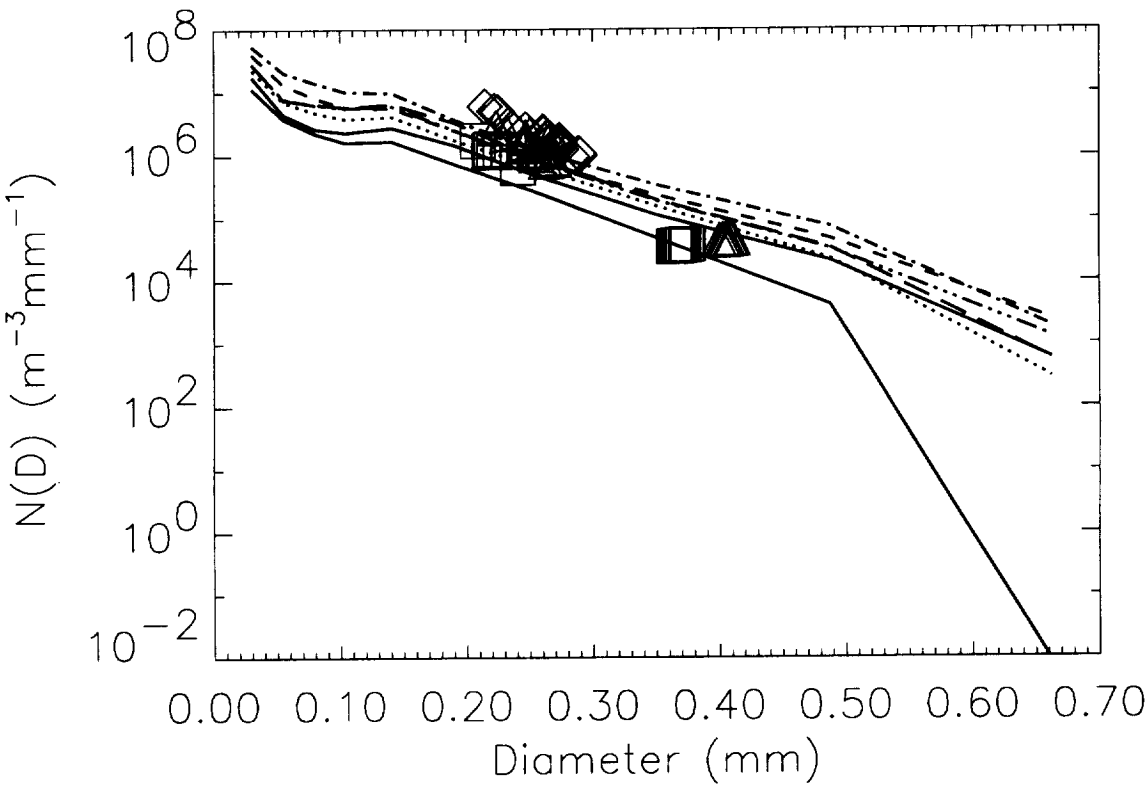

Figure 7: CAPAC in situ observations from the DC-8 at 12 km altitude for 14:00 to 14:06 UTC (lines) and retrieved anvil *N(D)* for $D = D_0$ at 11.5 km (diamond shapes), 12.0 km (triangles), and 12.5 km (squares).